In Situ TEM Observation of Fe-Included Carbon Nanofiber: Evolution of Structural and Electrical Properties in Field Emission Process

Mohd Zamri Mohd Yusop,[†,‡] Pradip Ghosh,[†] Yazid Yaakob,[†] Golap Kalita,[†,§] Masato Sasase,[⊥] Yasuhiko Hayashi,[†] and Masaki Tanemura[†,*]

[†]Department of Frontier Materials, Nagoya Institute of Technology, Gokiso-cho, Showa-ku, Nagoya, 466-8555 Japan, [‡]Department of Materials, Faculty of Mechanical Engineering, Universiti Teknologi Malaysia, 81310 UTM Skudai, Johor, Malaysia, [§]Center for Fostering Young and Innovative Researchers, Nagoya Institute of Technology, Gokiso-cho, Showa-ku, Nagoya, 466-8555 Japan, and [⊥]Wakasawan Energy Research Center, Nagayoshi-cho, Tsuruga-shi, Fukui, 914-0192 Japan

ABSTRACT *In situ* transmission electron microscopy (TEM) of single Fe-included carbon nanofibers (CNFs) revealed that the fine polycrystalline structure in the shank region of CNFs transformed to graphitic, hollow structures during a field emission (FE) process. The iron metal platelets agglomerated during the FE process and perceptibly were emitted from the shank, which featured bamboo-like carbon nanotube (CNT) structures. The structural evolution also improved the electrical properties, and the FE current was remarkably increased, that is, 1000 times higher than the initial value (from 10^{-9} to 10^{-6} A). The structural transformations were effectuated by Joule heating that generated simultaneously during the FE process. The *in situ* TEM study of room-temperature-synthesized CNFs could provide essential information regarding CNFs' structural transformation for their possible application in future electron emitter sources.

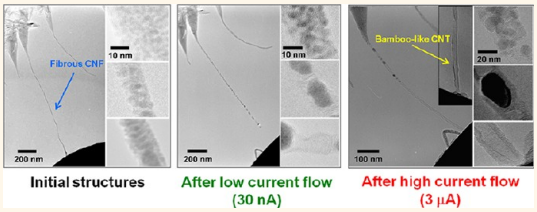

KEYWORDS: *in situ* TEM · field emission · ion-induced carbon nanofibers · graphitization · electromigration

One-dimensional carbon nanomaterials such as CNTs and CNFs are known to be essential for the next generation of FE emitters such as FE displays,[1−3] X-ray sources,[3,4] and electron imaging instruments,[5] due to their extremely sharp tips and high aspect ratios.[6−8] Much effort has been devoted to the fabrication of bulk CNTs/CNFs and theoretical works to achieve the most powerful and efficient emitters by controlling their morphology, structures, and growth conditions.[9−13] For understanding the FE phenomena of CNTs/CNFs, measurement of the FE properties of individual CNT/CNF while observing morphological and structural changes is highly indispensable.

In situ TEM of carbon nanomaterials has generated great interest. The detailed information from the TEM images potentially offers interpretations in nanoscale about carbon nanomaterial characteristics and prospective applications.[6,14,15] In the early stage of *in situ* TEM works, researchers successfully demonstrated the structural changes of CNTs by annealing treatment.[16−18] For example, Ichihashi *et al.* reported that Fe-doped amorphous carbon was transformed into graphitic tubules after annealing at 650−900 °C.[18] They observed that the metal particles remained at the tip of the CNT and that the graphitic structure was not aligned with the axial direction of the CNT. In that report, unfortunately, the electrical property of transformed nanotubes was not dealt with. Wang *et al.* observed that the FE process effectively modified the tip structure of CNTs.[19] The FE properties also appeared to be highly dependent on the cap structures of CNTs.[20−22] However, *in situ* TEM results of CNF and their field emission properties have rarely been reported.[23]

In our recent work, we demonstrated that single pristine CNFs were able to maintain stable FE properties for more than 30 min without remarkable current fluctuation and

* Address correspondence to tanemura.masaki@nitech.ac.jp.

Received for review June 25, 2012 and accepted October 9, 2012.

Published online October 09, 2012
10.1021/nn302889e

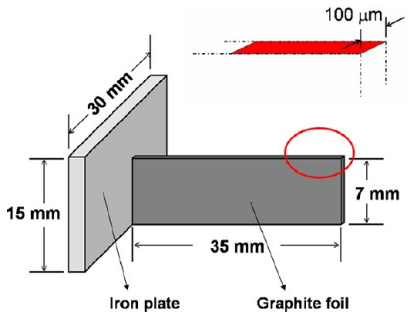

Figure 1. Sample setup for the synthesis of Fe-included CNFs. Inset shows marked area where CNFs were used for *in situ* TEM observation.

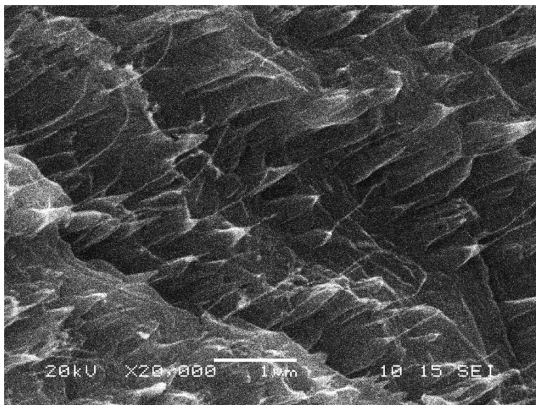

Figure 2. SEM image of the morphology of Fe-included CNFs at graphite edge after Ar^+ ion bombardment. Note that Fe-included CNFs grew toward the ion beam directions.

observed the transformation of the polycrystalline CNF to an onion-ring-like graphitized structure.[23] Recently, we observed also the dramatic change in crystalline structure from fine polycrystalline Cu−carbon composite fiber to a CuO_2 nanowire covered with graphene layers by current flow (direct current by applying small bias voltage) for a Cu-included CNF.[24] On the basis of our previous reports, we considered that it would be very interesting to investigate the change in crystalline structure and the effect on the FE property of metal-included CNFs. In this paper, we tackled this subject for Fe-included CNFs.

RESULTS AND DISCUSSION

Figure 2 shows the SEM image of Fe-included CNFs after ion irradiation. It should be noted that only a single Fe-included CNF grew on each respective cone and no Fe-included CNF grew without cone bases.[25] Figure 3a−d shows the TEM images of Fe-included CNFs. The Fe-included CNFs usually vibrate during TEM observation due to thermal vibration.[26] However, we overcame this difficulty simply by contacting the nanoprobe tip with the tip of the Fe-included CNF. The Fe-included CNF was approximately 1170 nm in length and 13 nm in diameter (Figure 3a). Figure 3b−d shows the high-magnification fibrous structures of the Fe-included CNF at the cone, shank, and fiber tip parts, respectively, revealing the dispersion of fine Fe crystallites in the

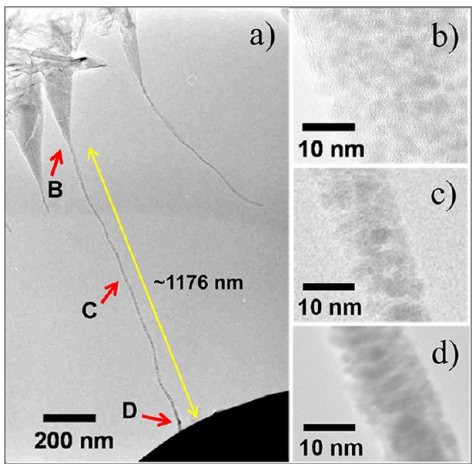

Figure 3. (a) TEM image of the intact structure of Fe-included CNF before the FE process. (b−d) High-magnification TEM images of the regions indicated by arrows B (cone), C (shank), and D (tip) in panel a, respectively, showing fine Fe crystallites dispersed in amorphous carbon matrix. Scale bars in (b−d) indicate 10 nm.

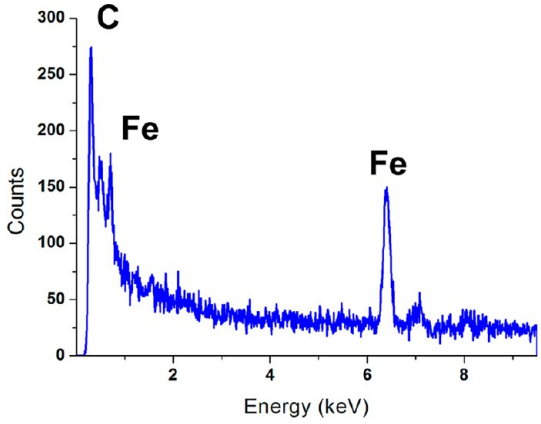

Figure 4. EDS spectra of the fiber part of the Fe-included CNF before FE measurement, disclosing that it was composed of Fe and C.

amorphous carbon matrix. Figure 4 shows the energy-dispersive X-ray spectrometry (EDS) spectra, which indicated that the Fe-included CNFs are mainly composed of carbon and iron.

To investigate the structural transformation of Fe-included CNFs by the FE process, we performed both the low (nanoampere range) and high (microampere range) emission current flows on an Fe-included CNF. For the low and high emission current measurements, maximum voltages applied were 150 and 180 V, respectively, with incremental steps of 10 V. The sample was observed at ×30k magnification in TEM. The gap distance between the gold-coated tungsten nanoprobe (anode) and the Fe-included CNF tip (cathode) was approximately 2.16 μm. The pressure in the specimen chamber was about 10^{-5} Pa during the FE measurement. FE properties were measured twice at low and high emission current flows. Every time, voltages were applied to the Fe-included CNF and its structure

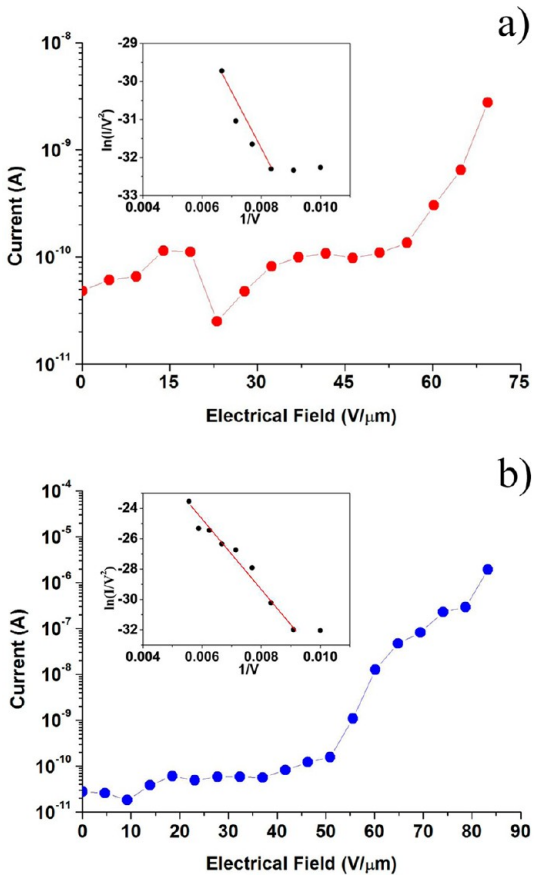

Figure 5. FE plot (current (nA) *versus* electrical field (V/μm)) of the Fe-included CNF of the (a) low current and (b) high current properties. Insets show the F−N plots for low and high current properties, respectively.

was found to be bent toward the anode due to the charge effect generated by the applied electric field.[27]

Figure 5a shows the plot of current *versus* applied electrical field after applying low voltage on the Fe-included CNF (Figure 3). In this case, the highest current flow was observed to be around 30 nA at 70 V/μm. Figure 6a−d shows the corresponding TEM images that were obtained after the measurement of low emission current properties. Figure 6a reveals the formation of the Fe-included CNF after applying a low voltage through the FE process. From a comparison between Figures 3 and 6, it should be noticed that the FE process induced Joule heating under a high electrical field and initiated the Fe platelets to agglomerate and form into bigger Fe particles (Figure 6c). The Joule heating also induced the transformation of thin graphitic layer structure from the amorphous carbon (Figure 6d). Due to the low current flow (~30 nA), structural transformation was only limited at the shank and tip parts of the Fe-included CNF, as shown in Figure 6. Figure 6b shows the high-magnification TEM image at the cone part after low current properties measurement, which indicates almost no major transformation.

Figure 5b shows the plot of the electric field *versus* current with the highest emission current flow of around 2.0 μA at 83 V/μm. FE property can be analyzed

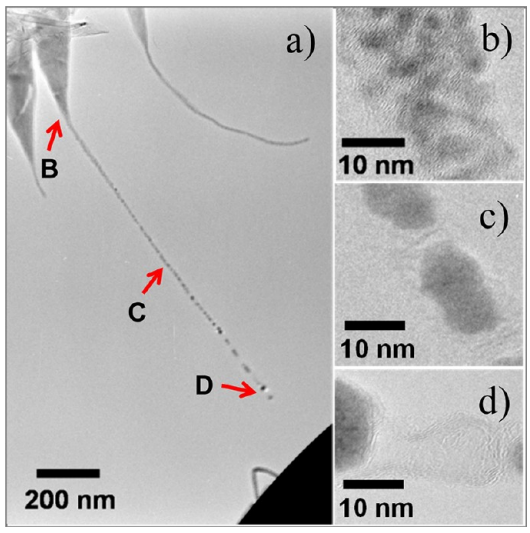

Figure 6. TEM images of the Fe-doped CNF structure after low current properties measurement. (a) Low-magnification TEM image. (b−d) High-magnification TEM images of the regions indicated by arrows B (cone), C (shank), and D (tip) in panel a, respectively, showing the structural transformation after low current flow. Scale bars in (b−d) indicate 10 nm.

using Fowler−Nordheim (F−N) equation[28]

$$I = \frac{k_1 A F^2}{\phi} \exp\left(-k_2 \frac{\phi^{3/2}}{F}\right)$$

where $k_1 = 1.54 \times 10^{-6}$ A eV V^{-2} and $k_2 = 6.83 \times 10^9$ eV$^{-3/2}$ V m^{-1}. I is the emission current, and A is the emission area; ϕ is the work function in electronvolts. The local electrical field F is usually proportional to voltage V

$$F = \frac{\beta V}{d}$$

where β is the field enhancement factor and d is the gap distance between the anode and cathode (CNF). By assuming a work function of 4.6 eV for graphite, β was calculated to be 73.6 from the slope of the F−N plot. This value is almost comparable to that reported for single CNTs in short gap distance (~2 μm) configuration.[22,29]

Figure 7a−d shows the TEM images of the Fe-included CNF after applying a high current on it. High emission current flow induced a more significant structural transformation than low emission current flow. During the high emission current flow, the original fibrous structure of the Fe-included CNF was transformed into graphitic hollow structures, as shown in Figure 7a. The inset of Figure 7a shows the bamboo-like structure of the Fe-included CNF after a high current flow. The flow of electrons would cause the Fe particles to migrate (electromigration)[30,31] and finally to eject from the shank into a vacuum. Moreover, the graphitic structure formation was also accelerated by Joule heating[32] under a high electrical field.[23] Figure 7b,c shows that only a few Fe particles remained inside the

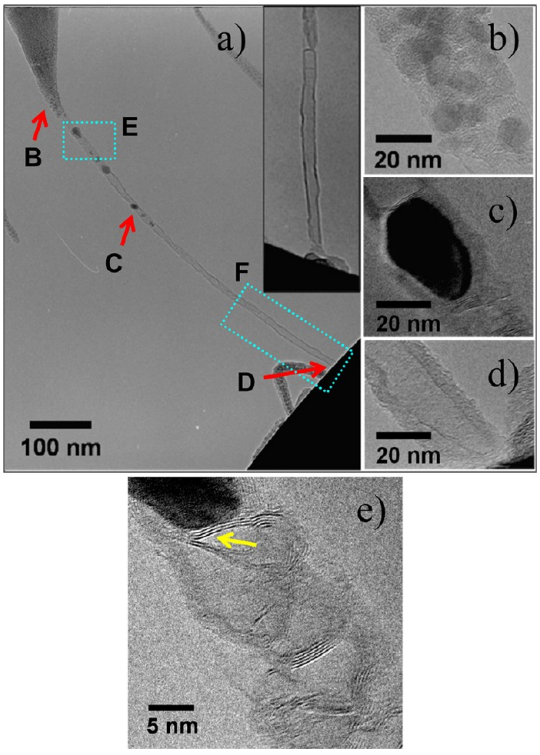

Figure 7. TEM images of the Fe-doped CNF structure after high current properties measurement. (a) Low-magnification TEM image. Inset shows a magnified image of the region indicated by rectangle F. (b–d) High-magnification TEM images of the regions indicated by arrows B (cone), C (shank), and D (tip) in panel a, respectively, revealing the structural transformation after high current flow. Scale bars in (b–d) indicate 20 nm. (e) High-magnification TEM image of the region indicated by rectangle E, showing the formation of graphitic layers (indicated by the arrow).

CNF shank and cone. The carbon diffusion enhanced by Joule heating would lead the tip part to the hollow structure with a closed end, as shown in Figure 7d. When the metals were emitted from the interior, they would cause the tip structure to open up; however, the open end would close during the FE due to the process of self-repair of the emitting CNT.[19,20,33] Figure 7e shows the graphitic layers (shown by arrow) over Fe particles in the shank part. As seen in Figure 7d, after the emission of Fe particles, the graphitized closed end tapered at the tip. Since the electric field is higher at the sharper tip, this would be the reason why the emission current increased after the emission of Fe particles. Figure 8a–c schematically explained the formation of hollow structure, inner graphitic layers, and agglomeration of Fe platelets during the FE process. The initial structure of Fe-included CNF was a fibrous structure filled by Fe platelets of dissimilar sizes and amorphous C, as shown in Figure 8a. The Joule heat that was generated during the FE process induced the Fe platelets to agglomerate into bigger particles, and simultaneously, an interfacial diffusion of carbon atoms through Fe particles produced graphene layers around the Fe particles, as shown in Figure 8b. Finally, the Fe particles migrated and emitted through the shank of the CNF by electromigration, leaving the inner wall with a bamboo-like CNT structure.

Later on, we investigated the electrical performance improvement for another Fe-included CNF before and after structural evolution. We chose the Fe-included CNF with similar characteristics to the previous one, and a constant voltage (230 V) was applied on it at the same gap distance (2.1 μm) as before. Image recording

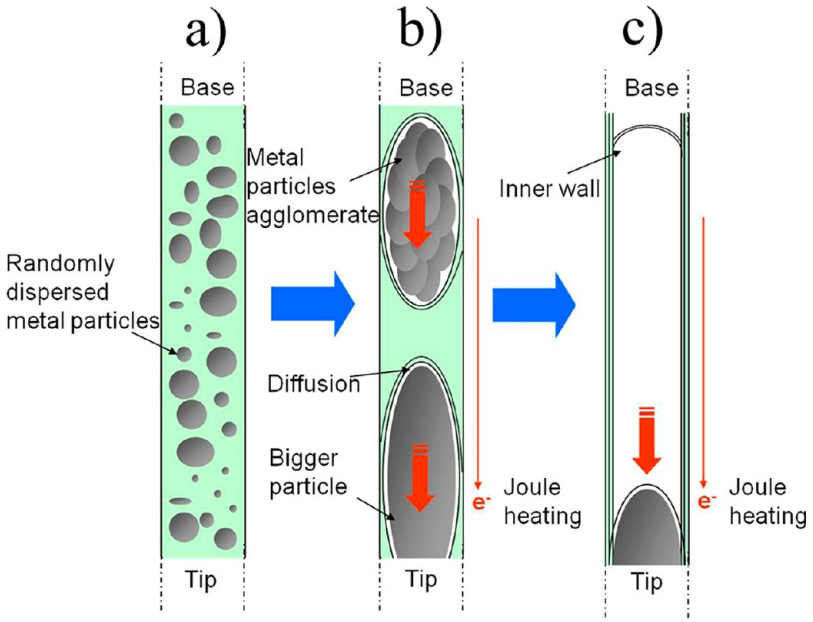

Figure 8. Schematic diagram of the formation process of bamboo-like CNT structures during high current flow. (a) Initial structure of Fe-included CNF, (b) Joule-heat-induced agglomeration of Fe platelets into bigger particles and formation of graphene layers around Fe particles through carbon diffusion, and (c) Fe particle migration due to electromigration, forming bamboo-like CNT structures.

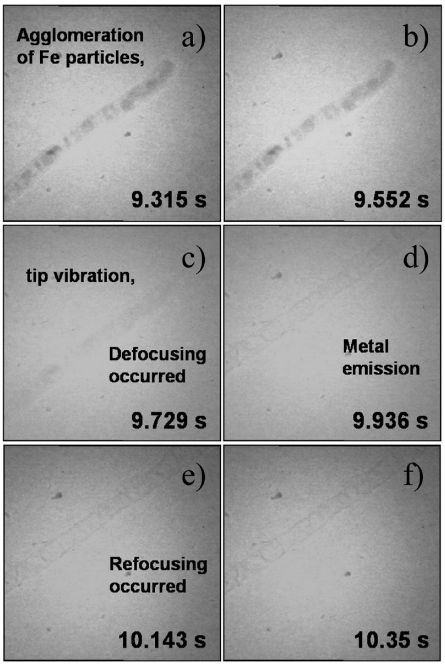

Figure 9. Sequence of structural transformations of an Fe-included CNF during the FE process under a constant applied field (applied voltage: 230 V), with elapsed time. (a) Agglomeration of Fe particles. (b) Fiber started to vibrate and (c) defocusing occurred due to the strong vibration of the fiber. (d) Emission of Fe particles through the shank, leaving a hollow structure. (e) After the emission of Fe particles, refocusing occurred and (f) transformation into bamboo-like CNT structures was clearly observed.

and applied voltage application were started at the same time. The dynamic transformational image recording was performed by charge-coupled devices (Picolo Series, Picolo), and the exposure time was set at around 0.5 to 1.5 s per frame. Figure 9a–f shows TEM images of the instantaneous transformation of Fe-included CNF to bamboo-like CNT during the FE process. We found that, during Fe particle emission through CNF's shank, the CNF was defocused due to the vibration of Fe particles, as shown in Figure 9d. The structure also indicates that the Fe-included CNF's length was elongated by the Fe particles' emission. Figure 9f shows the images of the bamboo-like CNT structure refocused after Fe emission. The emission

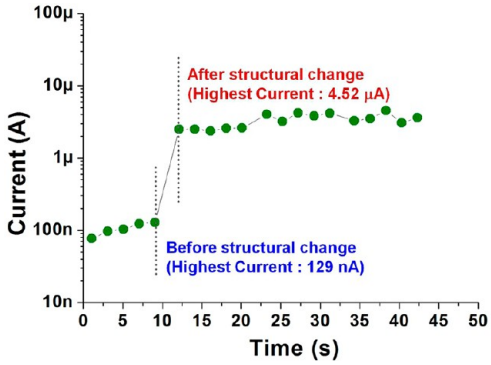

Figure 10. Current properties (current (A) *versus* time (s)) of the Fe-included CNF under the constant applied field, corresponding to Figure 9. Before the structural change, the highest emission current was 129 nA. After the structural change, the emission current increased to 4.52 μA.

current was significantly increased after the structural transformation (Figure 10), during the FE process. Before structural transformation, the current was 129 nA and increased to 4.52 μA after structural transformation during the FE process. The increment of the current properties during the FE process was considered to be affected by the crystallization process and the stretching of the structure (increment of the length would increase the aspect ratio).

CONCLUSIONS

In summary, the FE-induced structural change of Fe-included CNFs fabricated on the edge of a graphite foil was observed by *in situ* TEM. The FE properties of the single Fe-included CNF showed the highest current of 2.0 μA. After those FE measurements, dramatic change in the Fe-included CNF structure was observed from the fibrous amorphous and/or very fine crystallites, to the graphitic hollow structure. The fibrous and amorphous nature of the Fe-included CNF was transformed to a hollow graphitic structure, and the Fe particles incorporated into the CNF moiety were migrated and emitted to the vacuum through the CNF shank during the FE process. The FE process which released Joule heating was considered to be responsible for the structural transformation of the Fe-included CNFs.

METHODS

We used a Kaufmann-type ion gun (Iontech. Inc. Ltd., model 3-1500-100FC) for growing CNFs. Samples employed were commercially available graphite foils with a dimension of 5 mm $\times$ 10 mm $\times$ 100 μm. The edges of the foils were irradiated with argon ions (Ar^+) at room temperature. The growth mechanism of ion-induced CNFs was explained elsewhere in detail.[34] In brief, the growth mechanism of ion-induced CNFs can be described as follows: Ion irradiation on the surface creates conical protrusions due to the initial surface roughness, grain orientation, grain boundary, crystalline defect, *etc.* In this process, the sputter-ejected carbon atoms redeposit onto the sidewall of the conical protrusions. Also, the redeposited carbon atoms diffuse toward the tips, and finally, CNFs are formed. For the growth of Fe-included CNFs, an additional Fe plate, 15 mm $\times$ 10 mm, was vertically placed adjacent to the graphite foil as a source of Fe and was co-irradiated with Ar^+ ion at 45° from normal to the surface for 45 min at room temperature, as shown in Figure 1. The oblique Ar^+ bombardment is known to be more suitable for the growth of ion-induced CNFs than the normal incidence.[35] The diameter and ion beam energy employed for this experiment were 6 cm and 1 keV, respectively. The basal and working pressures were 1.5 $\times$ 10^{-5} and 2.0 $\times$ 10^{-2} Pa, respectively.

After sputtering, the morphology of the Fe-included CNFs grown on the edge of the graphite foils was carefully observed

by scanning electron microscope (SEM (JEOL JSM-5600)), and the crystallinity of the sample was examined by TEM (JEOL JEM-3010 and JEOL JEM-3000F (for video observation)). We used a TEM sample holder (JEOL; EM-Z02154T) with a piezo-controlled tungsten nanoprobe coated with gold to verify the current–voltage ($I-V$) characteristics of the single Fe-included CNF sample. The sputtered graphite foil was cut into small sizes of 2 mm width and directly mounted on the TEM sample holder without any additional post-treatment to observe the structure and crystallinity of Fe-included CNFs.

Conflict of Interest: The authors declare no competing financial interest.

Acknowledgment. This work was partially supported by a grant from the Wakasawan Energy Research Center and the Japan Society for the Promotion of Science (JSPS; Grants-in-Aid for Scientific, Research B, Grant No. 23360020).

REFERENCES AND NOTES

1. Ghosh, P.; Zamri, M. Y.; Satoh, S.; Subramanian, M.; Hayashi, A.; Hayashi, Y.; Tanemura, M. Transparent and Flexible Field Electron Emitters Based on Conical Nanocarbon Structures. *J. Am. Chem. Soc.* **2010**, *132*, 4034–4035.
2. Jung, Y. J.; Kar, S.; Talapatra, S.; Soldano, C.; Viswanathan, G.; Li, X.; Yao, Z.; Ou, F. S.; Avadhanula, A.; Vajtai, R.; *et al.* Aligned Carbon Nanotube-Polymer Hybrid Architectures for Diverse Flexible Electronic Applications. *Nano Lett.* **2006**, *6*, 413–418.
3. Connolly, T.; Smith, R. C.; Hernandez, Y.; Gun'ko, Y.; Coleman, J. N.; Carey, J. D. Carbon-Nanotube-Polymer Nanocomposites for Field-Emission Cathodes. *Small* **2006**, *5*, 826–831.
4. Kawakita, K.; Hata, K.; Sato, H.; Saito, Y. Development of Microfocused X-ray Source by Using Carbon Nanotube Field Emitter. *J. Vac. Sci. Technol., B* **2006**, *24*, 950–952.
5. Tan, T. T.; Sim, H. S.; Lau, S. P; Yang, H. Y.; Tanemura, M.; Tanaka, J. X-ray Generation Using Carbon-Nanofiber-Based Flexible Field Emitters. *Appl. Phys. Lett.* **2006**, *88*, 103105/1–103105/3.
6. de Jonge, N.; Lamy, Y.; Schoots, K.; Oosterkamp, T. H. High Brightness Electron Beam from a Multi-walled Carbon Nanotube. *Nature* **2002**, *420*, 393–395.
7. Nilsson, L.; Groaning, O.; Emmenegger, C.; Kuetell, O.; Schaller, E.; Schlapbach, L.; Kind, H.; Bonard, J. M.; Kern, K. Scanning Field Emission from Patterned Carbon Nanotube Films. *Appl. Phys. Lett.* **2000**, *76*, 2071–2073.
8. de Heer, W. A.; Châtelain, A.; Ugarte, D. A Carbon Nanotube Field-Emission Electron Source. *Science* **1995**, *270*, 1179–1180.
9. Zhang, Y.; Zou, G.; Doorn, S. K.; Htoon, H.; Stan, L.; Hawley, M. E.; Sheehan, C. J.; Zhu, Y.; Jia, Q. Tailoring the Morphology of Carbon Nanotube Arrays: From Spinnable Forests to Undulating Foams. *ACS Nano* **2009**, *3*, 2157–2162.
10. Shang, N.; Papakonstantinou, P.; Wang, P.; Zakharov, A.; Palnitkar, U.; Lin, I. N; Chu, M.; Stamboulis, A. Self-Assembled Growth, Microstructure, and Field-Emission High-Performance of Ultrathin Diamond Nanorods. *ACS Nano* **2009**, *3*, 1032–1038.
11. Kim, Y. C.; Nam, J. W.; Hwang, M. I.; Kim, I. H.; Lee, C. S.; Choi, Y. C.; Park, J. H.; Kim, H. S.; Kim, J. M. Uniform and Stable Field Emission from Printed Carbon Nanotubes through Oxygen Trimming. *Appl. Phys. Lett.* **2008**, *92*, 263112/1–263112/3.
12. Zhao, B.; Futaba, D. N.; Yasuda, S.; Akoshima, M.; Yamada, T.; Hata, K. Exploring Advantages of Diverse Carbon Nanotube Forests with Tailored Structures Synthesized by Supergrowth from Engineered Catalysts. *ACS Nano* **2009**, *3*, 108–114.
13. Smith, R. C.; Silva, S. R. P. Maximizing The Electron Field Emission Performance of Carbon Nanotube Arrays. *Appl. Phys. Lett.* **2009**, *94*, 133104/1–133104/3.
14. Wang, Z. L.; Gao, R. P.; de Heer, W. A.; Poncharal, P. *In Situ* Imaging of Field Emission from Individual Carbon Nanotubes and Their Structural Damage. *Appl. Phys. Lett.* **2002**, *80*, 856–858.
15. de Jonge, N.; Allioux, M.; Oostveen, J. T.; Teo, K. B. K.; Milne, W. I. Low Noise and Stable Emission from Carbon Nanotube Electron Sources. *Appl. Phys. Lett.* **2005**, *87*, 133118/1–133118/3.
16. Yuzvinsky, T. D.; Mickelson, W.; Aloni, S.; Begtrup, G. E.; Kis, A.; Zettl, A. Shrinking a Carbon Nanotube. *Nano Lett.* **2006**, *6*, 2718–2722.
17. Jung, S. I.; Jo, S. H.; Moon, H. S.; Kim, J. M.; Zang, D. S.; Lee, C. J. Improved Crystallinity of Double-Walled Carbon Nanotubes after a High-Temperature Thermal Annealing and Their Enhanced Field Emission Properties. *J. Phys. Chem. C* **2007**, *111*, 4175–4179.
18. Ichihashi, T.; Fujita, J.; Ishida, M.; Ochiai, Y. *In Situ* Observation of Carbon-Nanopillar Tubulization Caused by Liquid-like Iron Particles. *Phys. Rev. Lett.* **2004**, *92*, 215702/1–215702/4.
19. Wang, M. S.; Wang, J. Y.; Peng, L. M. Engineering the Cap Structure of Individual Carbon Nanotubes and Corresponding Electron Field Emission Characteristics. *Appl. Phys. Lett.* **2006**, *88*, 243108/1–243108/3.
20. Doytcheva, M.; Kaiser, M.; de Jonge, N. *In Situ* Transmission Electron Microscopy Investigation of the Structural Changes in Carbon Nanotubes during Electron Emission at High Currents. *Nanotechnology* **2006**, *17*, 3226–3233.
21. Asaka, K.; Nakahara, H.; Saito, Y. Nanowelding of a Multi-walled Carbon Nanotube to Metal Surface and Its Electron Field Emission Properties. *Appl. Phys. Lett.* **2008**, *92*, 023114/1–023114/3.
22. Xu, Z.; Bai, X. D.; Wang, E. G.; Wang, Z. L. Field Emission of Individual Carbon Nanotube with *In Situ* Tip Image and Real Work Function. *Appl. Phys. Lett.* **2005**, *87*, 163106/1–163106/3.
23. Zamri, M.; Ghosh, P.; Hayashi, A.; Hayashi, Y.; Tanemura, M.; Sasase, M. Structural Change of Ion-Induced Carbon Nanofibers by Electron Current Flow. *J. Vac. Sci. Technol., B* **2011**, *29*, E103–E107.
24. Zamri, M.; Ghosh, P.; Wang, Z. P.; Kawagishi, M.; Hayashi, A.; Hayashi, Y.; Tanemura, M. Direct Growth of Carbon Nanofibers on Metal Mesh Substrates by Ion Irradiation Method. *J. Vac. Sci. Technol., B* **2010**, *28*, C2C9–C2C12.
25. Tanemura, M.; Okita, T.; Tanaka, J.; Kitazawa, M.; Itoh, K.; Miao, L.; Tanemura, S.; Lau, S. P.; Yang, H. Y.; Huang, L. Room-Temperature Growth and Applications of Carbon Nanofibers: A Review. *IEEE Trans. Nanotechnol.* **2006**, *5*, 587–594.
26. Hafner, J. H.; Cheung, C. L.; Oosterkamp, T. H.; Lieber, C. M. High-Yield Assembly of Individual Single-Walled Carbon Nanotube Tips for Scanning Probe Microscopies. *J. Phys. Chem. B* **2001**, *105*, 743–746.
27. Rinzler, A. G.; Hafner, J. H.; Nikolaev, P.; Lou, L.; Kim, S. G.; Tomanek, D.; Nordlander, P.; Colbert, D. T.; Smalley, R. E. Unraveling Nanotubes: Field Emission from An Atomic Wire. *Science* **1995**, *269*, 1550–1553.
28. Fowler, R. H.; Nordheim, L. Electron Emission in Intense Electric Fields. *Proc. R. Soc. London, Ser. A* **1928**, *119*, 173–181.
29. Smith, R. C.; Cox, D. C.; Silva, S. R. P. Electron Field Emission from a Single Carbon Nanotube: Effects of Anode Location. *Appl. Phys. Lett.* **2005**, *87*, 103112/1–103112/3.
30. Regan, B. C.; Aloni, S.; Ritchie, R. O.; Dahmen, U.; Zettl, A. Carbon Nanotubes as Nanoscales Mass Conveyors. *Nature* **2004**, *428*, 924–927.
31. Begtrup, G. E.; Gannett, W.; Yuzvinsky, T. D.; Crespi, V. H.; Zettl, A. Nanoscale Reversible Mass Transport for Archival Memory. *Nano Lett.* **2009**, *9*, 1835–1838.
32. Asaka, K.; Karita, M.; Saito, Y. Graphitization of Amorphous Carbon on a Multiwall Carbon Nanotube Surface by Catalyst-Free Heating. *Appl. Phys. Lett.* **2011**, *99*, 091907/1–091907/3.
33. de Jonge, N.; Doytcheva, M.; Allioux, M.; Kaiser, M.; Mentink, S. A. M.; Teo, K. B. K.; Lacerda, R. G.; Milne, W. I. Cap Closing of Thin Carbon Nanotubes. *Adv. Mater.* **2005**, *17*, 451–455.
34. Tanemura, M.; Okita, T.; Yamauchi, H.; Tanemura, S.; Morishima, R. Room-Temperature Growth of a Carbon

Nanofiber on the Tip of Conical Carbon Protrusions. *Appl. Phys. Lett.* **2004**, *84*, 3831–3833.
35. Tanemura, M.; Tanaka, J.; Itoh, K.; Fujimoto, Y.; Agawa, Y.; Miao, L.; Tanemura, S. Field Electron Emission from Sputter-Induced Carbon Nanofibers Grown at Room Temperature. *Appl. Phys. Lett.* **2005**, *86*, 113107/1–113107/3.